



# Study of *in vivo* brain glioma in a mouse model using continuous-wave terahertz reflection imaging

LIMIN WU,<sup>1,2</sup> DEGANG XU,<sup>1,2</sup> YUYE WANG,<sup>1,2,3,4</sup> BIN LIAO,<sup>3</sup> ZHINAN JIANG,<sup>1,2</sup> LU ZHAO,<sup>3</sup> ZHONGCHENG SUN,<sup>1,2</sup> NAN WU,<sup>3</sup> TUNAN CHEN,<sup>3,5</sup> HUA FENG,<sup>3</sup> AND JIANQUAN YAO<sup>1,2</sup>

<sup>1</sup>Institute of Laser and Optoelectronics, School of Precision Instruments and Optoelectronics Engineering, Tianjin University, Tianjin 300072, China

<sup>2</sup>Key Laboratory of Optoelectronic Information Science and Technology (Ministry of Education), Tianjin University, Tianjin 300072, China

<sup>3</sup>Department of Neurosurgery and Key Laboratory of Neurotrauma, Southwest Hospital, Third Military Medical University (Army Medical University), Chongqing 400038, China

<sup>4</sup>yuyewang@tju.edu.cn

<sup>5</sup>ctn@tmmu.edu.cn

**Abstract:** We demonstrated that *in vivo* brain glioma in a mouse model using a continuous-wave terahertz reflection imaging system, as well as the *ex vivo* fresh brain tissues in mouse model. The tumor regions of *in vivo* and *ex vivo* brain tissues can be well distinguished by THz intensity imaging at the frequency of 2.52THz. The THz images with high sensitivity correlated well with magnetic resonance, visual and hematoxylin and eosin stained images. Furthermore, the THz spectral difference between brain gliomas and normal brain tissues were obtained in the 0.6THz to 2.8THz range, where brain gliomas have the higher refractive indices and absorption coefficients, and their differences increase particularly in the high frequency range. These results suggest that THz imaging has great potential as an alternative method for the intraoperative label-free diagnosis of brain glioma *in vivo*.

© 2019 Optical Society of America under the terms of the [OSA Open Access Publishing Agreement](#)

## 1. Introduction

Brain gliomas are the most common and deadly malignant brain tumors [1]. It grows invasively and has unclear margins between the neoplastic and normal regions [2]. Even experienced surgeons cannot increase the rate of complete resection beyond 20% using white light microscopy [3]. There are many techniques have been employed to distinguish gliomas and demarcate accurate tumor margins. Generally, the tumor marker can be visualized using appropriate staining methods with an optical microscope, which is called gold standard [4]. Hematoxylin and eosin (H&E) staining can accurately identify tumor region, but it requires immobilized sections of the sample and is only suitable for *ex vivo* pathological analysis. Currently, gliomas can be identified *in vivo* by a neuronavigation system based on preoperative magnetic resonance imaging (MRI) and positron emission tomography (PET) imaging [5]. However, MRI often fails to trace tumor margins during the operation due to brain-shift and it is time-consuming and very expensive. Compared with MRI, PET imaging not only has lower resolution (about 2-3mm) but also requires injecting positron-emitting radionuclide into the body. Fluorescence imaging [6] has also been used to detect glioma during surgery, but this method needs dye administered preoperatively such as 5-aminolevulinic acid. This increases not only the burden on the patient but also sometimes stains normal tissues around the tumor. Therefore, more viable tools to help doctors better distinguish gliomas during operation are urgently wanted.

Terahertz (THz) wave imaging technology, based on the low energy, high water absorption, nonionization, and existence of characteristic spectrum for individual

substances [7], has been studied as one of the candidate technologies for medical imaging. To date, the researches on THz biological imaging have been extended to more than ten kinds of diseases, including various cancers [8,9], dermatology [10], oncology [11] and many other medical fields [12,13]. In neurosurgery field, THz spectra and imaging have been tried to reveal essential characteristics differences between tumor and normal tissues. Terahertz time domain spectroscopy (THz-TDS), capable of extracting both the amplitude and phase information of the pulsed terahertz signal simultaneously, was used to detect the difference of the absorption coefficient and refractive index for gliomas. In 2014, K. Meng et al. have demonstrated the spectral differences between paraffin-embedded brain gliomas and normal brain tissues in the 0.2 to 2.0THz range [14]. S. Yamaguchi et al. quantitatively described water content and cell density were the origin of differences in the refractive index between normal and tumor tissues using THz spectroscopy, where the fresh sliced sample and paraffin-embedded sample were measured in the 0.8 to 1.5THz range and 1.0 to 1.3THz respectively [15]. And analysis of gelatin-embedded human brain glioma of different grades has been carried out using the THz-pulsed spectroscopy [16]. Based on the THz-TDS system, THz imaging for brain tumor has also been reported. S. J. Oh et al. demonstrated that tumors in both freshly and paraffin-embedded excised whole brain tissues could be differentiated clearly from normal brain tissue using the peak to peak reflection ratio of THz signal in the 0.3 to 1.3THz range [17,18]. In 2016, S. Yamaguchi et al. proved the complex refractive index values can be used to discriminate between normal and tumor tissues of fresh rat brain tissue in the frequency range of 0.8 to 1.5 THz [19]. Moreover, THz images of excised human fresh brain tumor from grade II to IV gliomas have also been reported using the peak to peak reflection ratio of THz signal, and *in vivo* gliomas imaging of a living mouse was performed [20]. However, to date, these researches have mainly focused on the *ex vivo* samples and the THz frequency was limited below 2THz. To our knowledge, THz imaging of *in vivo* brain glioma with high THz frequency has not been demonstrated.

In this paper, the THz imaging of *in vivo* and *ex vivo* brain gliomas in mouse model have been presented based on continuous-wave THz reflection (TR) imaging system. The tumor regions in *in vivo* and *ex vivo* brain tissues can be well distinguished by THz intensity imaging. Moreover, the comparison among THz image, MR, visual and H&E-stained images was performed. The THz spectral differences between brain gliomas and normal brain tissues were obtained and analyzed in the frequency range of 0.6THz to 2.8THz, where both differences for refractive indices and absorption coefficients increased with the THz frequency. The results indicate that higher THz frequency shows good feasibility for *in vivo* and *ex vivo* brain glioma discrimination.

## 2. Methodology

### 2.1 Experiment setup

The schematic diagram of the homemade THz imaging system is shown in Fig. 1. An optically pumped THz gas laser (FIRL100, Edinburgh Instruments Ltd.) was used, which is capable of emitting high-power, tunable continuous THz wave. The THz frequency was chosen at 2.52THz with the maximum output power of 150mW. The Golay cells (GC-1P, Tydex Ltd.) were used as the detectors for THz wave. Considering the responsivity of the detectors, the THz wave output was modulated as a sinusoidal signal using a chopper operating at 50Hz. In order to reduce the image noises from slight power fluctuations, the THz wave was separated into two sub-beams by a wire grid polarizer (Microtech Instruments, Inc.). One sub-beam was used as the intensity reference to improve the SNR of THz imaging. The other sub-beam, which was collimated and guided by two gold-coated flat mirrors and four off-axis parabolic mirrors, reached the detector after reflection from the sample positioned in the THz beam path. The focal length of the parabolic reflectors was 2inch and the F-number was 1. The sample was located at the focus of the THz beam, and the reflection window made of quartz material was placed over the sample with contact pressure for

imaging, which was mounted on a computer controlled  $x$ - $y$  linear motor stages (SIGMA KOKI CO., LTD.). The scanning step was set as  $200\mu\text{m}$  in this study. The scanning speed is determined by the stage and approximated to  $10\text{pixels/s}$  in the present system. In order to avoid the error caused by the inhomogeneity of the reflection window, the image of nothing under the quartz plate, i.e. just a quartz/air interface, was taken as the image reference. The intensity of acquired pixel in images indicates the THz reflectance of biological tissues. In other words, THz reflectivity in images was calculated by dividing the THz signal of the reflection window with sample by the THz signal of the reflection window without sample. The resolution of this system was  $600\mu\text{m} \times 600\mu\text{m}$  measured by the knife-edge method. The experiment was done at a controlled room temperature.

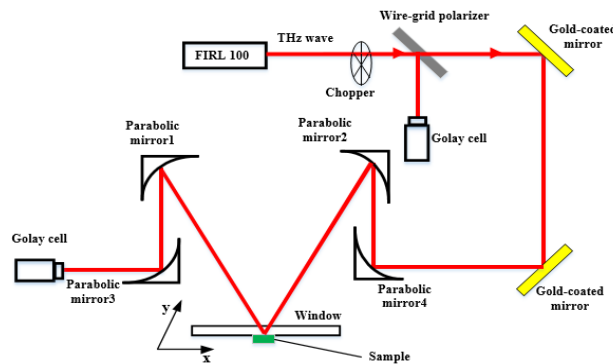


Fig. 1. Continuous-wave terahertz reflection imaging system.

To investigate the spectrum of brain tissue in the THz range, a commercially available THz time-domain spectroscopy (TDS, Advantest Corp., TAS7500SP) in transmission geometry was used. The spectrum reached over  $2.8\text{THz}$  from  $0.6\text{THz}$ . The frequency resolution and spatial resolution of this THz-TDS system are  $7.6\text{GHz}$  and  $2\text{mm}$ , respectively. The measurements were performed at room temperature ( $23^\circ\text{C}$ ) with dry air purge (almost  $0\%$  relative humidity).

## 2.2 Sample preparation

A reproducible measurement protocol is established by standardizing all experimental steps of sample preparations and THz measurements.

The brain tumor models for our study were an orthotopic glioma model of nude mice. This model has a clear boundary between the normal and tumor regions, in other words, the tumor can be well dissected from the normal tissue. U87-MG cell line was obtained from American Type Culture Collection (ATCC, Manassas, Virginia). A total of 36 5-week-old specific pathogen-free levels (SPF-level) BALB/c male mice weighing  $20 \pm 2\text{ g}$  were obtained from the Beijing Hua Fu Kang Biotechnology Limited Liability Company (Beijing HFK Bio-Technology.co., LTD). All animal experiments were performed in accordance with the China Animal Welfare Legislation, and were approved by the Third Military Medical University Committee on Ethics for the Care and Use of Laboratory Animals.

The samples were divided into three groups and used for *in vivo* imaging, freshly excised brain tissue imaging and spectrum measurement. The number of the sample with glioma in each group is 15, 15 and 6, respectively. For the comparison, the same surgical procedures are also performed on the normal mice for each group. There are other 5 normal mice in the *in vivo* and *ex vivo* imaging group. The glioma model was established by implanting U87-MG glioma cells into mice. Briefly, the mice were anesthetized with  $40\text{mg/kg}$  pentobarbital by intraperitoneal injection. The cell density was adjusted to  $8 \times 10^3\text{ cells}/5\mu\text{L}$  in serum-free Dulbecco's modified Eagle medium/nutrient mixture F-12 (DMEM/F12) culture medium and

then 5 $\mu$ L of the cell suspension was injected into the right caudate nucleus. The mice were placed on a stereotaxic instrument. After sterilization and skin incision, a 0.8mm diameter hole was made with a micro-electrical drill on the skull at a position of 2mm anterior from the posterior fontanel and 3mm lateral from the sagittal suture. Stereotaxic coordinates were taken from bregma and dura mater according to the mouse brain atlas. The mice were allowed to grow for 2-3 weeks and T2-weighted MR image was performed. For the sample of *in vivo* imaging, after MR image, a cranial window was made to expose the brain tumor. The surrounded blood and cerebrospinal fluid were sucked away by brain cotton slices. The *in vivo* sample was placed on the reflection window to obtain THz-TR image. Although such process causes some shift or extrusion for local tissue less than 1mm, it is acceptable in neurosurgical operations. Then, the mice were euthanized and their entire brains were removed immediately. The freshly excised brain tissues were quickly put to  $-15^{\circ}\text{C}$  slicing machine, and a thin section of 20 $\mu\text{m}$  thickness was sliced from the surface for histopathological examination by H&E staining. Thus, H&E-stained images were observed to compare with the THz image. For the sample of *ex vivo* imaging and spectrum measurement, the mice were directly euthanized and their brains were removed immediately prior to THz measurements. The extracted brains were divided evenly on the coronal surface with a scalpel. One part was for THz imaging or spectrum detection and the other part was quickly put to  $-15^{\circ}\text{C}$  slicing machine for freezing slice staining.

### 3. Results and discussion

To study the terahertz characteristics of *in vivo* brain tissue, we performed THz reflection imaging of *in vivo* brain samples. In our experiment, there are total 15 mice with glioma and 5 normal mice in this group. Visual, MR, TR and H&E-stained images for brain tissues with and without tumor were shown in Fig. 2. We used T2-weighted MR imaging to observe the condition of glioma *in vivo*. The tumor was observed for Nos. 1-3 samples, whereas there was no tumor for the No. 4 sample, as shown in Fig. 2(a). The brightness of the MR image in the tumor region with high signal was higher than that of the normal tissue, indicating that the water content in the tumor tissue was higher than that in the normal tissue [21]. The high signal was not found in the normal mouse (No. 4). After the MR scanning, we made a cranial window and exposed the brain tissue to obtain the THz image, as shown in Fig. 2(b). Figure 2(c) shows the THz images of *in vivo* brain tissues with and without tumor based on THz reflection imaging system. Each pixel was described using the THz reflectivity. Contrary to the imaging results of glioma in previous articles [17,18,20], the reflectance of glioma regions has a lower value than normal tissue in this paper. This is because the reflection window of destructive interference [22] at the detection wavelength was used for THz imaging. In fact, the tumor regions have higher reflectance than normal tissues without quartz window, which was consistent with previous articles. It is clearly seen that the THz reflection image for the normal mouse looks uniform, with the average reflectance of 60%. Terahertz image of glioma tissue showed obvious difference in tumor region compared with the normal tissue, as shown in the red region in Fig. 2(c). The average reflectance value of the abnormal region is about 50%, which is lower than that for the normal brain tissue. After the TR scanning, to verify the accuracy of THz image, the whole brain was extracted from the mouse and pathologically determined with the H&E-stained image, as shown in Fig. 2(d) and (f). The tumor region appeared paler in the visible images of frozen samples, which is marked by dashed lines in Fig. 2(d). In the H&E-stained image, the tumor region is recognized as an area with deep purple hematoxylin staining, corresponding that the cell nuclei density of tumor areas is higher than that of normal tissues. On the whole, the volume and location of the tumor region shown in the THz image are similar to those of the corresponding MR, visual and H&E-stained images. The little position and size shifts for the No. 3 sample can be attributed to the process of sample preparation, where the surfaces of the *in vivo* fresh tissue for THz image and H&E-stained sections were slightly different.

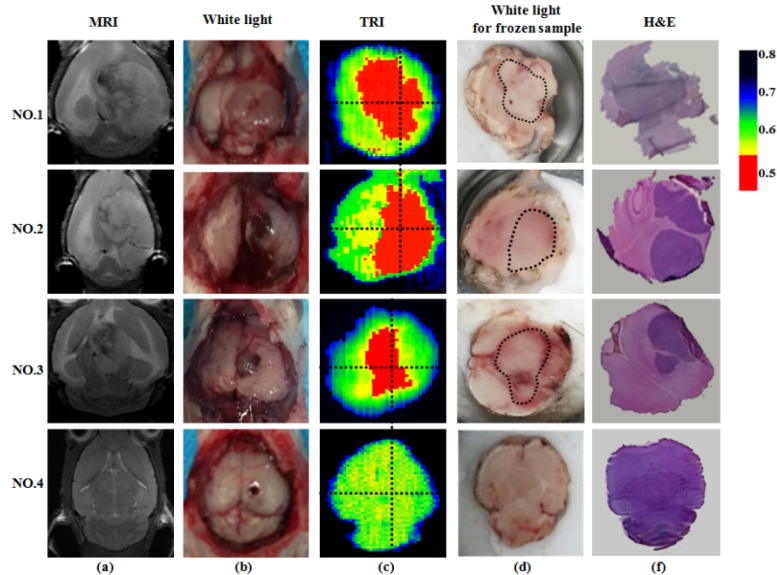


Fig. 2. (a) MR, (b) visual of *in vivo*, (c) THz reflection, (d) visual of fresh excised and (e) H&E-stained images of whole brain images with (Nos. 1–3) and without (No. 4) tumors.

Figure 3 shows the detailed profile of the reflectance values along the horizontal and vertical lines of Fig. 2(c). For the tumor tissue, the reflectance values of the tumor region was lower than 52%, whereas the reflectance values for the normal tissues was rarely lower than 52%. Considering all the *in vivo* samples, the dynamic range of the THz reflectance values for the normal and tumor tissues are  $54\% \pm 2\%$  and  $48\% \pm 3\%$ , respectively. Thus, the threshold value of 52% was chosen to differentiate tumor region from normal tissue in Fig. 2(c). The regions of the tumors in the THz images corresponded to those of real tumors, as shown in Fig. 2(a) and (d). The tumor signals were rarely found in the normal brain regions. These results indicate that THz imaging can realize *in vivo* brain glioma discrimination despite the brain is composed of many complicated components. Considering the result well agrees with the MRI and has a high sensitivity without any additional contrast agent, THz imaging technique could be a useful tool to determine the location of *in vivo* brain glioma and complement conventional radiological techniques.

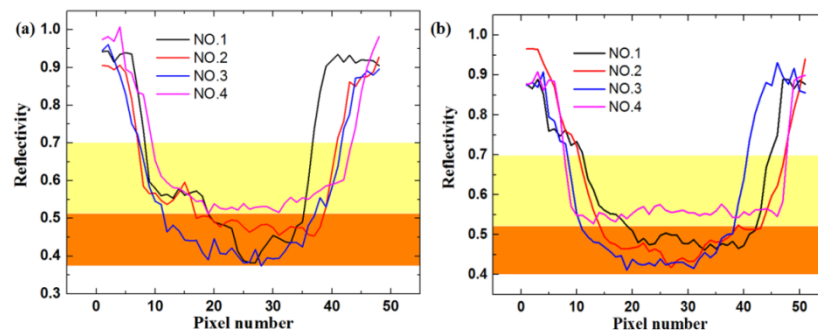


Fig. 3. THz reflectivity on the (a) horizontal, (b) vertical lines of Fig. 2(c).

In order to further confirm the glioma discrimination ability with THz wave, freshly excised brain tissues and dehydrated paraffin-embedded brain tissue have also been studied. A total of 15 freshly excised brain samples were tested, including 5 normal samples and 10 tumor samples. Figure 4(a) shows the MR image for the observation of samples without and

with gliomas *in vivo* (Nos. 5-8). After the MR scanning, the fresh specimens were extracted. Then, the samples were all pruned at  $-15^{\circ}\text{C}$  using a microtome until the transverse section match with MR images, as shown in Fig. 4(b). On one hand, the tissue was cut into uniform slices for H&E staining, indicated by Fig. 4(c). On the other hand, the adjacent sample part was used for TRI examination. Figure 4(d) shows the THz images of freshly excised brain tissues. The average THz reflectance value of the abnormal regions is about  $52\% \pm 2\%$ , whereas the average reflectance for the normal brain tissue is about  $57\% \pm 3\%$ . Thus, the tumor region can be distinguished from the normal tissue in the THz image. Compared to *in vivo* THz image, the average THz reflectance values for *ex vivo* samples increased a little. This can be attributed to the water dehydration during the processes of sample preparation and measurement. It is noted that the location of the tumor region shown in the THz image are similar to those in the corresponding MR, visual and H&E-stained images. Furthermore, we compare the tumor areas detected by MR, H&E staining and TR images. The estimated values of the tumor size for Nos. 6-8 samples are listed in Table 1. The size of abnormal regions indicated clearly by THz image was larger than those detected using MR ( $256 \times 256 \mu\text{m}^2$ ) and H&E-stained images. The relative low spatial resolution for TR ( $600 \times 600 \mu\text{m}^2$ ) image is one possible reason. Another possible reason is THz imaging could indicate the presence of perifocal edema around the tumor region. Generally, the water content increases in tumor tissue because angiogenesis occurs to compensate for the lack of oxygen and nutrients. Pathological changes in cellular metabolism will result in edema around the tumor region. Thus, there is high water content both inside and outside the cells in the perifocal edema area but cell density is essentially normal. As THz wave is sensitive to the distribution of water content and cellular hydration state [23], we speculate THz imaging may be able to reflect the edema around the tumor. As reported in Ref [24], the response of edema was similar to that of tumor in 0.2-1.5 THz frequency, the edema tissue around the tumor would be confused with tumor. This limitation may be overcome by the combination of THz imaging with other microscopic method at the cellular level in the clinical glioma surgery application.

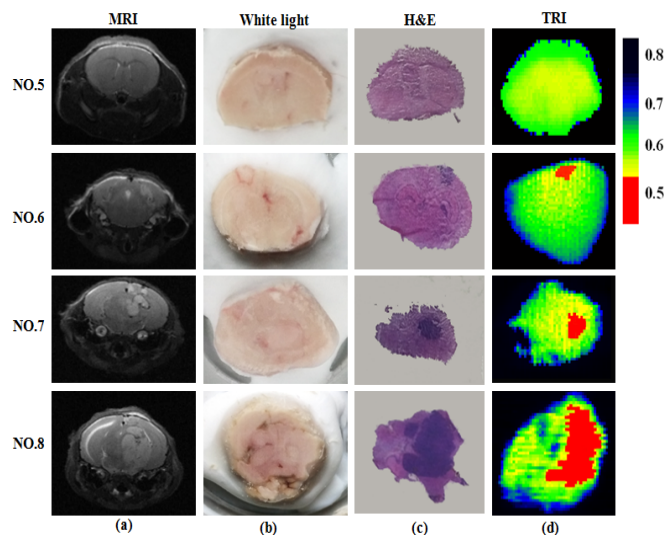


Fig. 4. (a) MR, (b) Visual, (c) H&E-stained and (d) terahertz reflection images of fresh excised brain tissues without (No. 5) and with (Nos. 6-8) tumors.

Table 1. Tumor Sizes of MR, Histological and TR Images

Mice no.	Tumor sizes (mm <sup>2</sup> )		
	MRI	H&E-stained image	RI
6	1.82	2.07	2.15
7	3.49	3.95	4.03
8	13.72	14.09	14.25

For the better understanding the characterization of the human U87-MG bearing mouse sample, the spectra of 6 fresh brain tumor samples were measured. Considering the spatial resolution of the THz-TDS system was 2mm, the mouse brain was horizontally sliced in the experiment to ensure that the light spot can totally cover the tumor region or normal region. In order to avoid water loss and other errors during sample measurement, the tissue with 60 $\mu$ m thickness was sandwiched by two quartz plates and wrapped with vaseline and oleic acid. The time-domain THz pulses were collected at three different spot in tumor area or healthy area for each sample. Every measurement point was repeatedly tested 3 times with the setting of 1024 times scan for each measurement. Due to the biological diversity, all spectra are averaged results of 6 samples and the standard deviation is shown as error bars.

Figure 5(a) shows the THz time-domain waveforms transmitted through glioma, normal brain tissue and the substrate without sample. The average amplitudes of brain tissues were smaller than those of the reference pulse. The amplitudes of the average spectra of the glioma were lower than those of the normal brain tissues. Then, a fast Fourier transform is used to obtain the frequency-domain spectra as shown in Fig. 5(b). Similarly, the amplitudes of the glioma were generally lower than those of the normal brains in the frequency domain ranging from 0.6THz to 2.8THz. As mentioned above, the water content increase in the tumor region is the dominant reason for the difference, which will affect the refractive index and absorption coefficient of tissue [25]. Figure 5(c) and Fig. 5(d) shows the refractive index spectra and the absorption coefficient spectra of normal and tumor regions in fresh tissues. It is clearly seen that the refractive index of tumor region is higher than that of normal tissue in the range from 0.6THz to 2.8THz and the inset of Fig. 5(c) show their difference values display a slight increase for higher frequencies. Consistently, the absorption coefficient of brain gliomas is higher than that of normal tissue in the 1.0-2.8THz range despite the error bars overlapped above 2.6THz, which is induced by the lower THz power together with high absorption. The difference of the absorption coefficients shows a distinct increase with the THz frequency increase, as presented in the inset of Fig. 5(d). Overall, it is reasonable to deduce that higher THz frequency is preferred for the THz imaging of brain glioma with better contrast on the condition of enough THz power. Additionally, the absolute reflectance for TR image was calculated using the complex refractive indices of tissue and quartz plate based on the TDS measurement, where destructive interference was considered [22]. The theoretical reflectance of tumor and normal tissues were 49% and 41% at 2.52THz, respectively. The difference value of 8% between tumor and normal tissues consists with that in TR images.

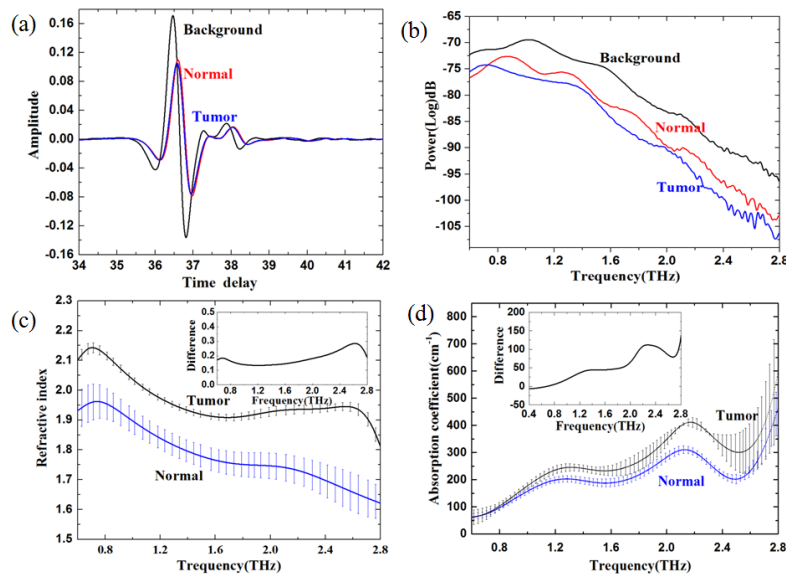


Fig. 5. (a) The THz-TDS signal, (b) the power, (c) the refractive index, and (d) the absorption coefficient of the freshly excised brain tissue samples. The insets of (c) and (d) show the difference of the refractive index and the absorption coefficient between tumor and normal tissue, respectively.

#### 4. Conclusion

We obtained THz reflection images of *in vivo* and *ex vivo* brain tissues without and with tumor from mice model by continuous-wave THz imaging system with 2.52THz. The tumor regions of mice brain tissue were diagnosed by THz intensity imaging and corresponded closely with MRI and H&E-stained images results. Besides, the refractive indices and absorption coefficients of freshly excised brain tissues have been measured by THz-TDS system in the 0.6 to 2.8THz range. The results show that higher THz frequency is preferred for the THz imaging of brain glioma. Therefore, high frequency THz intensity imaging has good capability to distinguish tumor regions. It would be worthwhile to further investigate the metastatic states of tumor and identify different grade gliomas. This might require better instrument performance in view of the high sensitivity of THz wave to the water content. Although this imaging methodology still needs improvements, particularly in imaging resolution and scanning time, our pilot study demonstration high frequency THz intensity imaging could be employed as a complementary technique allowing surgeons to determine tumor regions with a label-free and diagnostic imaging method in real time.

#### Funding

The National Basic Research Program of China (973) (2015CB755403); National Natural Science Foundation of China (NSFC) (61775160, 61771332); China Postdoctoral Science Foundation (2016M602954); Postdoctoral Science Foundation of Chongqing (Xm2016021); Joint Incubation Project of Southwest Hospital (SWH2016LHJC-04, SWH2016LHJC-01); The National Key Research and Development Projects under Grant (2016YFC0101001).

#### Disclosures

The authors declare that there are no conflicts of interest related to this article.

## References

1. E. G. Van Meir, C. G. Hadjipanayis, A. D. Norden, H. K. Shu, P. Y. Wen, and J. J. Olson, "Exciting new advances in neuro-oncology: the avenue to a cure for malignant glioma," *CA Cancer J. Clin.* **60**(3), 166–193 (2010).
2. Q. T. Ostrom, L. Bauchet, F. G. Davis, I. Deltour, J. L. Fisher, C. E. Langer, M. Pekmezci, J. A. Schwartzbaum, M. C. Turner, K. M. Walsh, M. R. Wrensch, and J. S. Barnholtz-Sloan, "The epidemiology of glioma in adults: a "state of the science" review," *Neuro-oncol.* **16**(7), 896–913 (2014).
3. M. Hefti, H. M. Mehdorn, I. Albert, and L. Dörner, "Fluorescence-guided surgery for malignant glioma: a review on aminolevulinic acid induced protoporphyrin IX photodynamic diagnostic in brain tumors," *Curr. Med. Imaging Rev.* **6**(4), 254–258 (2010).
4. M. Jansen, S. Yip, and D. N. Louis, "Molecular pathology in adult gliomas: diagnostic, prognostic, and predictive markers," *Lancet Neurol.* **9**(7), 717–726 (2010).
5. K. R. Swanson, G. Chakraborty, C. H. Wang, R. Rockne, H. L. P. Harpold, M. Muzi, T. C. H. Adamsen, K. A. Krohn, and A. M. Spence, "Complementary but distinct roles for MRI and 18F-Fluoromisonidazole PET in the assessment of human glioblastomas," *J. Nucl. Med.* **50**(1), 36–44 (2008).
6. W. Stummer, U. Pichlmeier, T. Meinel, O. D. Wiestler, F. Zanella, and H. J. Reulen; ALA-Glioma Study Group, "Fluorescence-guided surgery with 5-aminolevulinic acid for resection of malignant glioma: a randomised controlled multicentre phase III trial," *Lancet Oncol.* **7**(5), 392–401 (2006).
7. J. H. Son, "Terahertz electromagnetic interactions with biological matter and their applications," *J. Appl. Phys.* **105**(10), 102033 (2009).
8. Y. C. Sim, J. Y. Park, K. M. Ahn, C. Park, and J. H. Son, "Terahertz imaging of excised oral cancer at frozen temperature," *Biomed. Opt. Express* **4**(8), 1413–1421 (2013).
9. J. Y. Park, H. J. Choi, H. Cheon, S. W. Cho, S. Lee, and J.-H. Son, "Terahertz imaging of metastatic lymph nodes using spectroscopic integration technique," *Biomed. Opt. Express* **8**(2), 1122–1129 (2017).
10. R. M. Woodward, V. P. Wallace, R. J. Pye, B. E. Cole, D. D. Arnone, E. H. Linfield, and M. Pepper, "Terahertz pulse imaging of ex vivo basal cell carcinoma," *J. Invest. Dermatol.* **120**(1), 72–78 (2003).
11. C. B. Reid, A. Fitzgerald, G. Reese, R. Goldin, P. Tekkis, P. S. O'Kelly, E. Pickwell-MacPherson, A. P. Gibson, and V. P. Wallace, "Terahertz pulsed imaging of freshly excised human colonic tissues," *Phys. Med. Biol.* **56**(14), 4333–4353 (2011).
12. K. W. Kim, K.-S. Kim, H. Kim, S. H. Lee, J.-H. Park, J.-H. Han, S.-H. Seok, J. Park, Y. Choi, Y. I. Kim, J. K. Han, and J.-H. Son, "Terahertz dynamic imaging of skin drug absorption," *Opt. Express* **20**(9), 9476–9484 (2012).
13. S. Sung, S. Selvin, N. Bajwa, S. Chandra, B. Nowroozi, J. Garritano, J. Goell, A. Li, S. X. Deng, E. Brown, W. S. Grundfest, and Z. D. Taylor, "THz Imaging System for in vivo human cornea," *IEEE Trans. Terahertz Sci. Technol.* **8**(1), 27–37 (2018).
14. K. Meng, T. N. Chen, T. Chen, L. G. Zhu, Q. Liu, Z. Li, F. Li, S. C. Zhong, Z. R. Li, H. Feng, and J. H. Zhao, "Terahertz pulsed spectroscopy of paraffin-embedded brain glioma," *J. Biomed. Opt.* **19**(7), 077001 (2014).
15. S. Yamaguchi, Y. Fukushi, O. Kubota, T. Itsuji, T. Ouchi, and S. Yamamoto, "Origin and quantification of differences between normal and tumor tissues observed by terahertz spectroscopy," *Phys. Med. Biol.* **61**(18), 6808–6820 (2016).
16. N. V. Chernomyrdin, A. A. Gavdush, S. I. T. Beshplav, K. M. Malakhov, A. S. Kucheryavenko, G. M. Katyba, I. N. Dolganova, S. A. Goryaynov, V. E. Karasik, I. E. Spektor, V. N. Kurllov, S. O. Yurchenko, G. A. Komandin, A. A. Potapov, V. V. Tuchin, and K. I. Zaytseva, "In vitro terahertz spectroscopy of gelatin-embedded human brain tumors a pilot study," *Proc. SPIE* **10716**, 107160S (2018).
17. S. J. Oh, S. H. Kim, Y. B. Ji, K. Jeong, Y. Park, J. Yang, D. W. Park, S. K. Noh, S. G. Kang, Y. M. Huh, J. H. Son, and J. S. Suh, "Study of freshly excised brain tissues using terahertz imaging," *Biomed. Opt. Express* **5**(8), 2837–2842 (2014).
18. S. J. Oh, Y. M. Huh, S. H. Kim, J. Yang, K. Jeong, Y. Park, C. Kang, J. H. Son, and J. S. Suh, "Terahertz pulse imaging of fresh brain tumor," in *36th Int. Conf. on Infrared, Millimeter and Terahertz Waves (IRMMWTHz)* (2011).
19. S. Yamaguchi, Y. Fukushi, O. Kubota, T. Itsuji, T. Ouchi, and S. Yamamoto, "Brain tumor imaging of rat fresh tissue using terahertz spectroscopy," *Sci. Rep.* **6**(1), 30124 (2016).
20. Y. B. Ji, S. J. Oh, S. G. Kang, J. Heo, S. H. Kim, Y. Choi, S. Song, H. Y. Son, S. H. Kim, J. H. Lee, S. J. Haam, Y. M. Huh, J. H. Chang, C. Joo, and J. S. Suh, "Terahertz reflectometry imaging for low and high grade gliomas," *Sci. Rep.* **6**(1), 36040 (2016).
21. R. R. Edelman, J. R. Hesselink, and M. B. Zlatkin, *Clinical Magnetic Resonance Imaging*, Chap. 1 (Saunders, 1996).
22. H. Hirori, M. Nagai, and K. Tanaka, "Destructive interference effect on surface plasmon resonance in terahertz attenuated total reflection," *Opt. Express* **13**(26), 10801–10814 (2005).
23. Y. Y. Wang, T. Notake, M. Tang, K. Nawata, H. Ito, and H. Minamide, "Terahertz-wave water concentration and distribution measurement in thin biotissue based on a novel sample preparation," *Phys. Med. Biol.* **56**(14), 4517–4527 (2011).
24. A. A. Gavdush, N. V. Chernomyrdin, K. M. Malakhov, S. T. Beshplav, I. N. Dolganova, A. V. Kosyrkova, P. V. Nikitin, G. R. Musina, G. M. Katyba, I. V. Reshetov, O. P. Cherkasova, G. A. Komandin, V. E. Karasik, A. A.

- Potapov, V. V. Tuchin, and K. I. Zaytsev, "Terahertz spectroscopy of gelatin-embedded human brain gliomas of different grades: a road toward intraoperative THz diagnosis," *J. Biomed. Opt.* **24**(2), 1–5 (2019).
25. P. Wesseling, J. M. Kros, and J. W. M. Jeuken, "The pathological diagnosis of diffuse gliomas: towards a smart synthesis of microscopic and molecular information in a multidisciplinary context," *Diagn. Histopathol.* **17**(11), 486–494 (2011).